# Accurate deformation monitoring on bridge structures using a cost-effective sensing system combined with a camera and accelerometers: Case Study

Yan Xu[1], James M.W. Brownjohn[2], Farhad Huseynov[3,4]

[1]PhD student, Vibration Engineering Section, College of Engineering, Mathematics and Physical Sciences, University of Exeter, Exeter, EX4 4QF, UK

[2]Professor, Vibration Engineering Section, College of Engineering, Mathematics and Physical Sciences, University of Exeter, Exeter, EX4 4QF, UK

[3]Engineer, Full Scale Dynamics Ltd, North Park Road, Exeter, EX4 4QF, UK

[4]PhD student, School of Civil Engineering, University College Dublin, Dublin, Ireland

Abstract

Information on deformation is critical for bridge condition evaluation but accurate characterisation, usually via discrete displacement measurements, remains a challenging task. Vision-based systems are promising tools, possessing advantages of easy installation, low cost and adequate resolution in time and frequency domains. However, vision-based monitoring faces several field challenges and might fail to achieve the required level of working performance in some real-world test conditions e.g. involving low-contrast patterns and mounting instability of optical sensors. To make the best use of the potential of vision-based systems, a mixed sensing system consisting of a consumer-grade camera and an accelerometer is proposed in this study for accurate displacement measurement. The system considers automatic compensation of camera shake and involves autonomous data fusion process for noise reduction. The proposed system is demonstrated through a field monitoring test on a short-span railway bridge and is validated to offer higher accuracy and wider frequency range than using a camera alone. Displacement data by the mixed system are demonstrated to be viable for estimating bridge influence line, indicating the potential for bridge condition assessment.

Keywords:

Bridge deformation; bridge displacement; vision-based system; data fusion; Kalman filter.

## Introduction

Information on deformation is critical for bridge condition and performance assessment. It could reflect structural integrity, while extreme values in service might indicate the occurrence of abnormal loading or bridge deficiency. Pointwise deformation is deflection, and is measured as displacement of a point on a structure. When such measurements are made continuously and automatically over a period of time they are termed 'monitoring'.

Measurements of deflection on aging bridges under prescribed loads help to estimate their load carrying capacities (Wang et al. 2011) and could assist the owner decision-making process, for example regarding the need for expensive retrofitting. Knowledge of bridge deformation is also important for evaluating serviceability and for comparison of full-scale performance with predictions during the design process. Hence there are many motivations for accurate sensing approaches for bridge displacement monitoring.

### *Review of displacement sensing techniques*

Traditional contacting sensors such as linear variable differential transformers are usually impractical for full-scale monitoring due to the absence of a fixed reference point for relative displacement measurement. They are feasible only when the open space under a bridge deck is accessible, but they require a high installation effort (Moreu et al. 2015). Indirect measurement schemes using double integration of accelerometer data can work well for signals showing displacement patterns having periods up to ten seconds (Hester et al. 2017). However this approach may sometimes fail to recover displacement amplitude accurately due to low-frequency drift caused by the accumulation of measurement noise which is particularly noticeable for small displacements (e.g. lower than 1 mm). Instrumentation using the Global Positioning System (GPS) is commonly implemented for monitoring flexible bridges (e.g. long-span) since the range of their deformation in operation is compatible with the achievable GPS accuracy which is around the centimetre level (Casciati and Fuggini 2009; Nickitopoulou et al. 2006). Apart from accuracy (which differs from resolution), GPS performance is degraded during train passages (Moschas et al. 2013) and in cable-stayed or suspension bridges (Nickitopoulou et al. 2006) due to multi-path noise.

Remote sensing techniques for displacement monitoring include robotic total stations (RTS), vision-based systems, laser Doppler vibrometers (LDV) and radar interferometry. These sensors are easy to install with no dependence on a fixed reference point other than their own (stable) location. Access to a test structure is sometimes still either necessary or recommended for the installation of assistant tools such as reflective tapes for LDVs (Lou et al. 2017), reflective prisms for RTS (Brownjohn et al. 2015) and artificial targets for vision-based systems (Xu et al. 2016). Vision-based systems and radar interferometry both support multi-point simultaneous sensing, approaching true deformation monitoring, while distributions of test points in microwave interferometry systems are dependent on range resolution and less flexible.

Vision-based systems are the only type of remote sensing technique with potential to overcome the dependence on expensive commercial products, and are thus receiving increased attention. Another important advantage of vision-based monitoring is that a common error source induced by sensor mounting instability could possibly be corrected within the system itself.

Existing applications of vision-based systems for displacement monitoring in field tests cover a wide range of structural types including short-span bridges (Ehrhart and Lienhart 2015; Feng et al. 2015; Hoag et al. 2017), long-span bridges (Macdonald et al. 1997; Martins et al. 2015; Stephen et al. 1993; Xu et al. 2017), high-rise buildings (Liao et al. 2010) and stadium structures (Khuc and Catbas 2017). However, vision-based displacement monitoring faces several field challenges and might fail to capture the nature of the structural deformation due to site and environmental conditions e.g. camera and support motion induced by wind or human behaviours (Ribeiro et al. 2014), uncontrolled lighting variations due to cloud passing (Chen et al. 2017), low-contrast target patterns and pattern changes due to obstruction and rain drops (Brownjohn et al. 2017).

Although measurement accuracy of vision-based systems has been validated in some application examples (Ehrhart and Lienhart 2015; Feng et al. 2015; Khuc and Catbas 2017), the measurement quality is time-varying and environmentally dependent. Several undesired test conditions (e.g. camera shake, changes of tracking patterns and ambient lighting changes) could possibly reduce the measurement accuracy significantly. It is impossible to avoid all these unsatisfactory circumstances in

field testing and these influences are rarely considered in existing studies concerning the development of vision-based systems.

***Focus of this study***

The main purpose of this study is to investigate low-cost options for accurate displacement monitoring on bridge structures. To make the best use of the potential of vision-based systems, a mixed sensing system consisting of a consumer-grade camera and an accelerometer is proposed. Compared with vision-based systems described in existing literature, the displacement output from this mixed system considers the compensation of camera shake automatically and is capable of achieving a higher accuracy level and wider frequency bandwidth even for relatively low-contrast target patterns. Compared with similar work mixing vision-based systems with accelerometers (Chang and Xiao 2010; Park et al. 2018), the data fusion method used in this study (Xu et al. 2017) is an autonomous implementation without any user supervision or involvement. This mixed system could be implemented for applications where accurate and high-resolution displacement data are required and where the structure can be accessed e.g. for model calibration and estimation of vehicle weights. In this study, the measured displacement is interpreted for estimating a bridge influence line effectively by field measurement.

The proposed system is demonstrated through a field monitoring test on a short-span railway bridge during the passing of several trains, leading to a discussion about its working performance. The undesired test conditions considered include apparent camera shake and low-contrast patterns while the evaluation criterion is the accuracy level in the time domain. Although the data fusion method has the capacity to widen the frequency bandwidth of the estimated displacement time histories, capturing bridge dynamics is not the focus here. This is because traffic-induced deformations for road and railway bridges are always dominated by static and quasi-static components, while the dynamic components with relatively low signal-to-noise ratios are easily contaminated by measurement noise. Therefore, bridge dynamic information is better suited to measurement using accelerometers.

Since direct access to bridge structures is necessary for accelerometer installation in this mixed system, there is a kind of trade-off between having a high accuracy level and the benefit of non-contact sensing. When the signal-to-noise ratio is acceptable, the consumer-grade camera in this mixed system could be

used separately for completely non-contact and multi-point displacement (deformation) measurement in bridge applications. The performance of a single consumer-grade camera system is also evaluated in the field monitoring test.

The following five sections present system methodologies, one bridge demonstration test, test results in different monitoring conditions and discussion of data interpretation potential (i.e. for influence line estimation).

## Methodologies

This section describes the main methodologies implemented in the proposed mixed system, including the development of a vision-based system for displacement monitoring and the data fusion approach for merging displacement and collocated acceleration data.

### *Vision-based displacement monitoring*

The vision-based system developed for displacement monitoring in this study consists of a consumer-grade camera (GoPro Hero 4) for video recording and a post-processing package programmed in C++ for video analysis. The main algorithms have been reported in Xu et al. (2018) and the difference in this study is that the influence of camera shake is considered automatically within the calculation process.

The basic steps for extracting structural displacement from video records are localising target regions in image sequences and transforming image location information into structural displacement. Target tracking is one critical step in the video processing, with a few techniques available in literature e.g. correlation-based template matching (Feng et al. 2015), optical flow estimation and feature point matching (Ehrhart and Lienhart 2015). Correlation-based template matching is used in this study mainly for two reasons: (i) compared with other alternatives, the method has little dependence on user intervention except an initial selection of regions of interest (ROI) as the template and thus is suitable for automatic monitoring without any parameter adjustment; and (ii) the method achieves better resolution, especially for tracking low-contrast patterns (Xu and Brownjohn 2018). The template matching method is sensitive to background and lighting changes, thus for long-duration recording (e.g. over several hours), it is necessary to update the ROI template periodically to mitigate error accumulation. The similarity criterion used is zero-mean normalised cross-correlation coefficient and

the interpolation scheme is zero-padding in the frequency domain, using matrix multiplication involving the two-dimensional discrete Fourier transform (Guizar-Sicairos et al. 2008).

A detailed flowchart of the video processing procedure is provided in Fig. 1 including three main steps: camera calibration, target tracking and displacement calculation. In the camera calibration step, lens distortion parameters are calibrated in the laboratory ahead of field testing using a chessboard pattern with known dimensions. Projection distortion is often observed on site due to the optical line of sight not being perpendicular to the plane of motion of structural components. To consider the projection distortion, a transformation matrix (i.e. planar homography) is determined, assisted by some control points with known geometric information. Based on the point correspondences between structural coordinates of these control points and image coordinates of their projections, the projection transform is estimated using least-squares optimisation to the total re-projection error. The control points used for calibration could be edge points of pre-installed artificial targets or points from bridge components with known dimensions.

In the second step, correlation-based template matching is used to localise the ROIs in video frame sequences. To consider lens distortion influence, one feasible way is to correct video frames before the tracking step, but this is computationally very expensive. In the method used here, the correction occurs not to the full frame but only to the image coordinates estimated from raw frames, saving computational efforts.

When apparent frame shake is observed, a reference ROI around adjacent stationary objects visible in the frame e.g. foundation walls or bridge towers is also tracked. The camera motion is then compensated by subtracting the nominal motion of this reference target. This method has been implemented in several existing studies (Feng and Feng 2017; Murray et al. 2015; Yoneyama and Ueda 2012) and the difference in this study is that an automatic evaluation process for camera mounting condition is added to determine the necessity of camera motion correction. Two parameters are used to evaluate camera motion occurrence, i.e. the root means square (RMS) and the maximal value of the tracked motions for the stationary target as shown in Fig. 2. Tracking accuracy using correlation-based template matching method varies from 0.01 pixel to 0.08 pixel depending on target patterns through an evaluation study in laboratory conditions (Xu and Brownjohn 2018) and might become poorer in field testing. An

appropriate threshold for the image motion RMS is 0.05 pixel, considering the low-contrast feature of stationary natural targets. The maximum threshold is implemented on time series of the image motion after low-pass filtering to avoid the influence of abnormal events (e.g. sudden partial obstruction on targets), and the threshold is set as 0.08 pixel.

Finally, the two-dimensional structural displacement is derived based on image coordinates of the ROIs and the projection transform matrix.

***Data fusion of displacement and acceleration measurement***

Displacement and acceleration measurements have complementarity in sensing accurately low-frequency and high-frequency ranges respectively, and their integration leads to a better displacement estimation than from each measurement alone. Previous efforts of integrating displacement and acceleration data could be summarised into two categories: (i) by superimposition of two displacement data series (i.e. displacement measurement and integrated displacement from acceleration measurement) covering complementary frequency bands (Hong et al. 2013; Park et al. 2018); and (ii) by solving state space models based on kinematic equations using Kalman filter (KF) estimation (Chang and Xiao 2010; Kim et al. 2014; Li and Chang 2013; Smyth and Wu 2007; Xu et al. 2017).

In the superimposition method, complementary filter pairs are designed to take the desired displacement components from two displacement data series. This is actually the superimposition of 'reliable' components separately from two data series instead of creating a more reliable estimate from data redundancy. The working performance is dependent on certain parameters like the target frequency (the lowest frequency of dynamic displacement) for signal filtering (Hong et al. 2013).

A KF-based method could link displacement and acceleration measurements autonomously based on kinematic equations that have been widely implemented for the fusion of GPS and inertial measurement unit signals in the field of navigation (Sukkarieh 2000). For civil applications, the multi-rate Kalman filter method was originally proposed to fuse the measured acceleration and displacement signals with different sample rates (Smyth and Wu 2007) and then implemented for a footbridge displacement monitoring test (Chang and Xiao 2010). Instead of depending on frequency-selective filters, the estimation process using KF finds the best estimate at each time series recursively through a weighted average between the predicted state (based on the previous best estimate) and the new observation. The

relative weight given to the predicted and measured states (i.e. Kalman gain) is related to the uncertainty in the process and observational models hence selection of noise parameters has a direct influence on the estimation accuracy. Unfortunately these parameters are actually unknown in practice, but an approach based on maximum likelihood estimation (MLE) (Xu et al. 2017) was proposed to estimate the unknown parameters (i.e. covariances of the process and measurement noise) required by the multi-rate KF estimation. This was validated on GPS monitoring data from a long-span bridge.

The KF estimation enhanced by the MLE is implemented for data fusion in this study. A brief description is given here with full details given by Xu et al. (2017). The flowchart is illustrated in Fig. 3 including two main steps, the MLE for the parameter tuning and the KF for the displacement refinement. The MLE is an optimisation process to find the values of unknown parameters $\boldsymbol{\theta}$ in a statistical model that maximises the likelihood of this model given the observational data. The unknown parameters $\boldsymbol{\theta}$ here correspond to the noise variances of measured acceleration and displacement as well as the initial state of state variables (i.e. displacement and velocity). The deduced optimum $\boldsymbol{\theta}^*$ is used in the KF estimation step together with the state space model and measured displacement and acceleration data. The displacement estimates are deduced using the forward Kalman filter and then refined by backward smoothing.

Displacements output by the proposed mixed system are the results of the fusion of displacement data from a single camera and the collocated accelerometer measurement. A field monitoring test on a short-span railway bridge performed for system validation is reported in the next section.

## Field test on a railway bridge

This section describes a field monitoring test on a railway bridge for train-induced displacement measurement.

The Mineral Line Bridge shown in Fig. 4 is a skew steel girder bridge with the span length of 14.7 m (from a bridge reconstruction drawing), carrying the West Somerset Railway near Watchet in the UK. A single day of field measurements on 5$^{th}$ September 2017 was used to monitor the deformation induced by passing trains.

Three sensing systems were involved in this test, as indicated in Fig. 4 (b), including one consumer-grade camera (GoPro Hero 4), a commercial vision-based system (Imetrum dynamic monitoring system, DMS) and two accelerometers, all located in the north side of bridge. The test aimed to evaluate the effectiveness of two systems (i.e. a consumer-grade camera system and a mixed system combining a consumer-grade camera and accelerometers) for accurate displacement sensing through comparison with the reference sensor (Imetrum DMS).

GoPro Hero 4, a consumer-grade camera (cost ~$400) was mounted on a portable tripod stand, 6.9 m from the mid-span of the bridge. The frame rate was set as nominally 24 Hz and the image resolution was 1920 × 1080 pixels. A narrow field of view setting was selected with the corresponding focal length equivalent to 30-34 mm. The recorded video files initially stored in the camera flash memory card were copied to a computer for the post-processing to extract displacement time histories.

The Imetrum DMS is a commercial vision-based monitoring system developed by Imetrum Limited, UK and comprises one GigE professional camera and a controller containing a real-time video processing software Video Gauge (VG) for video acquisition and analysis. The Imetrum camera equipped with 50 mm focal length lens was arranged on site adjacent to the GoPro camera. As shown in Fig. 4 (b), a surveyor's tripod was used for the Imetrum camera, being more stable than the portable tripod stand for the GoPro camera. The frame rate was 30 Hz and the image resolution was 2048 × 1088 pixels. The auto-exposure feature was switched on in VG software for the automatic adjustment of exposure according to real-time lighting condition to ensure brightness consistency in selected target regions. The Imetrum DMS has been evaluated on several short-span and long-span bridge monitoring tests providing reliable and accurate measurements (Hester et al. 2017; McCormick et al. 2014; Xu et al. 2017), and displacement resolution was found to approach 0.1 mm in a field of view of 20 m (McCormick et al. 2014). Thus, the Imetrum DMS is used as the reference sensor in this study. It is noted that, however, the goal of the proposed mixed system is not to achieve similar performance as this commercial product (Imetrum DMS), but to overcome some general limitations faced by any vision-based system. Stable working performance of the Imetrum DMS was ensured in this study via a high quality tripod and the camera auto-exposure function for brightness consistency in selected target regions. Thus, the Imetrum measurements in this study fortunately avoided the undesired test conditions

discussed later for the GoPro measurement, i.e. apparent camera shake and low-contrast patterns. The mixed sensing system is also applicable to improve accuracy of the Imetrum measurements with less than perfect test conditions.

The QA-750 accelerometers are DC-response devices with a resolution better than 1 μg and sensor noise floor of 7 $\mu g / \sqrt{\text{Hz}}$ in 0-10 Hz band. The two uniaxial accelerometers located vertically were attached to the bridge's top flange using magnets at approximately mid-span and one-quarter span points, and the sample rate for data acquisition was set to 512 Hz.

The daytime records (lasting seven hours) include the passages of nine trains in total. Considering one train passing the bridge in less than 40 seconds approximately every 50 minutes, monitoring systems took records only around train passages based on the train timetable. The Imetrum system has a remote controller to start/stop video acquisition, thus the camera was not touched during whole recording periods except when adding a waterproof covering to protect against light rain. The GoPro camera was switched on/off by manually pressing one control button thus the camera position could possibly change slightly between different runs. Three runs of measurement data involving passing trains are presented in this study and the information is summarised in Table 1. Trains passing in Run 1 and 2 are of similar type consisting of one steam locomotive and eight carriages. The difference between the two runs is that the GoPro mounting arrangement was stable in Run 1 while apparent camera shake is observed in Run 2. Run 3 corresponds to the records during the passage of a diesel multiple unit train comprising three carriages but no locomotive. The maximum bridge deflection at the mid-span was approximately 3 mm, less than half the maximum deflection in Run 1 and 2, thus requiring higher measurement resolution. GoPro records in Run 3 also include the influence of considerable camera motion.

The measurement data in Run 1 are presented first to demonstrate the working performance of a sole camera system in a desired test condition (i.e. stable camera mounting and no observable change of target patterns). The data in Run 2 and 3 are used to validate the effectiveness of improving poor data due to camera motion and low-contrast target patterns through fusion with acceleration data.

## Displacement monitoring using a sole camera

This section demonstrates displacement information extraction from video files recorded using the consumer-grade GoPro camera. The measurement accuracy of a sole camera system through tracking both the artificial and natural targets in Run 1 is evaluated by comparison with the Imetrum DMS reference data.

### *Video processing process for GoPro records*

One sample frame in a GoPro video is indicated in Fig. 5(a) that includes apparent image distortion e.g. the parapet railings appear slightly bent. The lens distortion parameters were pre-determined in the laboratory and were used to remove lens distortion influence with the corrected frame in Fig. 5(b).

The step of camera calibration also involves estimating projection transformation (i.e. planar homography) through existing dimensions projected in the corrected frame. The geometric information used for calibration is from the width and height of artificial targets (T10 and T20 in Fig. 5(a)) attached to the bridge girder, both 200 mm. The planar homography matrices were estimated separately for the mid-span and one-quarter span targets using least-squares optimisation according to point correspondences.

In the second step of target tracking, a few regions of interest (ROIs) indicated in Fig. 5(a) were selected for analysis. The ROIs T10 and T20 are artificial targets with diffuse concentric ring patterns at the mid-span and one-quarter span of the bridge that were tracked by both the GoPro system and the Imetrum DMS. The measurement outputs by the two vision-based systems are compared to evaluate the GoPro system measurement. The ROIs T11 and T21 are natural feature targets including rivet patterns adjacent to the artificial targets. They were analysed in GoPro system to evaluate the feasibility and accuracy level for measuring structural features when direct access to the bridge is not available. The ROI T00 is one natural feature target located at the surface of the stationary masonry wall foundation and was tracked for correcting undesired camera shake when necessary. The ROI locations in the raw frame were estimated using a correlation-based template matching algorithm and then transformed to image coordinates in the corrected frame to consider lens distortion influence.

The tracking results for the ROI T10 along the image height direction during a train passage in Run 1 are shown in Fig. 6: the left and right axes correspond to the derived locations in the image plane before and after lens distortion correction, respectively. The main difference between two time-history signals is the relative location in the image plane instead of motion amplitudes. This indicates that lens distortion correction step is not essential when using a scaling factor to convert the target motion in the image plane to structural displacement. However, this step is necessary when other types of projection transformation (e.g. planar homography or full projection matrix) are implemented, since the target location sequences in the image plane are taken for structural displacement calculation.

To evaluate the camera mounting stability condition, the stationary region T00 was tracked, with the results indicated in Fig. 7. The RMS of the image motion (raw) along the image height direction is 0.035 pixel while the maximum deviation after the low-pass filter (with the cut-off frequency of 1 Hz) is 0.056 pixel. Since they are both within the threshold range, the step of camera motion correction is skipped.

Finally, the two-dimensional bridge displacement along the vertical and longitudinal directions were calculated based on the output of the camera calibration and target tracking steps.

***Displacement measurement in Run 1***

The train that passed the bridge in Run 1 consisted of a locomotive and a tender followed by eight carriages. Fig. 8 and Fig. 9 indicate the measured displacement in the vertical direction at mid-span and one-quarter span during the train passage.

At the mid-span of the bridge (Fig. 8), the maximum displacement induced by the locomotive at approximately 6.8 s is measured as 6.87 mm by the Imetrum DMS, 6.77 mm and 6.84 mm by the GoPro system tracking artificial (T10) and natural (T11) targets, respectively. Taking the measurement by the Imetrum DMS as the reference, the cross-correlation coefficients for the GoPro measurement reach 99.8% and 99.4% for tracking the artificial and natural feature targets, respectively. The measurement error for the GoPro is presented in Fig. 8 (b) through subtracting the reference (after interpolation to the same sample rate) with the root mean squares (RMS) of 0.11 mm and 0.22 mm.

At one-quarter span (Fig. 9), the maximum displacement measurement during the locomotive passage is 4.83 mm by the Imetrum DMS, 4.90 mm and 4.77 mm by the GoPro system for artificial (T20) and

natural (T21) targets, respectively. The cross-correlation coefficients between the GoPro measurement and the reference (by the Imetrum DMS) are 99.9% and 99.5%, respectively for tracking artificial target and natural feature patterns. Evaluated against the reference, the RMS of measurement difference using the GoPro system is quantified as 0.09 mm and 0.11 mm. This is slightly reduced compared with that at mid-span, probably due to the decreased distance to the camera.

Measurement noise during the stationary periods (including the first four seconds and the last five seconds) is evaluated using the root mean square (RMS) of measured data and the results are indicated in Table 2. Compared with the Imetrum DMS, the measurement results using the GoPro camera system include a larger noise level when tracking the same artificial targets (T10 and T20). The noise range could be more than doubled (with the RMS reaching 0.16 mm) when the tracked targets are less distinctive e.g. using the natural features (T11 and T21). This phenomenon is accordant with the application preference of high-contrast patterns in digital image correlation field (Schreier et al. 2009). The measurement noise at mid-span is slightly larger than that at one-quarter span possibly due to the increased camera-to-target distance.

Results indicate that the GoPro system alone could provide accurate measurement of train-induced bridge displacement. If direct access to the bridge is not allowed, the system is capable of performing non-contact displacement monitoring through tracking existing natural patterns with the noise RMS at approximately 0.2 mm, 2.9% of the displacement amplitude (6.8 mm).

Although the effectiveness of the GoPro system for accurate displacement measurement has been demonstrated in this section, the undesired circumstances for vision-based systems, like camera shake and very low-contrast patterns, were fortunately avoided during the monitoring period. It is hard to ensure this satisfactory working performance for every similar monitoring exercise since the uncontrolled circumstances mentioned above often affect measurement accuracy, leading to a much higher noise level.

**Displacement monitoring using a mixed system**

The purpose of this section is to examine the performance of a mixed monitoring system comprising a GoPro camera and accelerometers for accurate displacement sensing under unsatisfactory conditions

including considerable camera shake and poorer tracking resolution due to low-contrast patterns. This section implements the data fusion method on test data from Run 2 and 3 to evaluate the effectiveness of accuracy improvement compared to direct measurement using (only) a single camera with and without correction for camera shake.

***Data fusion process***

The GoPro measurement runs selected for data fusion involve considerable camera motion (concluded through evaluating 'nominal' image motions of the stationary target T00 following the procedure detailed in Fig. 2) that should be compensated in these two runs. The estimation process for extracting the mid-span displacement in Run 2 is demonstrated here. The image motions of the mid-span target T10 along the image height direction are presented in Fig. 10. The time history curve labelled 'T00' corresponds to the nominal motions of a stationary target (shifted by 0.5 pixel for clarification in the figure) located at the bridge foundation wall. The ROI T00 is expected to stay fixed during the whole recording period but actually experiences some high-frequency oscillations in both the first and last ten seconds as well as a considerable shift at 26 seconds. These effects could be attributed to the influence of camera shake and are used to correct the measurement at the ROI T10. The curve with the legend 'T10 (corrected)' represents the image motions of the target T10 after compensating the camera motion influence through subtracting the nominal motion of the stationary ROI T00.

Before the data fusion, the time shift between the QA accelerometer and the GoPro system is corrected by maximising the cross-correlation coefficients of the two time-history signals i.e. double-integrated displacement from the accelerometer data and the GoPro measurement after interpolation to the sample rate of accelerometer data (512 Hz). The two signals after the time synchronisation are indicated in Fig. 11.

The data fusion of acceleration and displacement measurement in this study includes two main steps, the MLE for parameter tuning and Kalman filter for displacement estimation. In the MLE step, the noise variances of acceleration and displacement data are deduced through an optimisation process. For the measured data at mid-span shown in Fig. 11, the standard deviation of measurement noise for the

accelerometer is estimated to be 0.002 $m/s^2$ while that for the GoPro displacement data is 0.22 mm. These results will be used in the Kalman filter estimation step to derive a refined displacement estimate.

***Displacement estimates in Run 2***

Fig. 12 (a) indicates displacement measurement and estimates in the vertical direction for the artificial target T10 at bridge mid-span during the passage of a steam train in Run 2. The two signals with the labels of 'Raw' and 'Corrected' correspond to the displacement measurement by the GoPro system without and with camera motion compensation, respectively. The signal labelled 'Corrected + Fusion' represents the displacement estimate by fusing the acceleration data and the GoPro displacement data ('Corrected'). The maximum displacement induced by the steam locomotive is measured as 6.51 mm by the reference sensor Imetrum DMS while the maximum values in these three signals are 7.30 mm ('Raw'), 6.50 mm ('Corrected') and 6.32 mm ('Corrected + Fusion'). The cross-correlation coefficients of these three signals compared with the reference are 97.0% ('Raw'), 98.6% ('Corrected') and 99.8% ('Corrected + Fusion'). The measurement differences evaluated through subtracting the reference data (interpolated to the same sample rate) are illustrated in Fig. 12 (b) with the RMSs at 0.53 mm ('Raw'), 0.30 mm ('Corrected') and 0.21 mm ('Corrected + Fusion'), respectively. Although the displacement data after correction ('Corrected') achieves a similar value of the maximum displacement as the reference, the fusion process could effectively reduce the high-frequency noise, providing displacement data ('Corrected + Fusion') with a higher cross-correlation coefficient evaluated against the reference. The captured maximum displacement after data fusion has larger deviation (0.19 mm or 2.9%) compared with the reference but is still acceptable for the purpose of normal bridge monitoring.

Comparison results for the displacement data at T11 (the natural target at bridge mid-span) and at T20 (the artificial target at bridge one-quarter span) are presented in Table 3. For the target T11, the displacement estimates involving camera motion correction and data fusion process have cross-correlation coefficient of 99.7% and the measurement difference RMS of 0.24 mm evaluated against the Imetrum reference.

For the target T20, the displacement estimates ('Corrected + Fusion') have the cross-correlation coefficient at 99.9% and the RMS at 0.05 mm for the measurement difference evaluated by the reference measurement.

Observations from Fig. 12 and Table 3 indicate that

- Camera shake could contaminate the measurement provided by a vision-based system and deserves attention in field monitoring tests. It is always preferable to implement a rigid camera mounting configuration and choose solid locations with the proper shelter for the tripod set-up.
- Camera motion correction through tracking the nominal motion of an adjacent stationary object is effective to remove the low-frequency drift, improving the measurement accuracy of vision-based systems. However, the measurement resolution might be reduced when tracking the low-contrast feature target on stationary parts for correction.
- Data fusion method through fusing with the collocated accelerometer data is capable of de-noising the displacement measurement and providing better estimates about bridge displacement.

Analysis results have validated the viability of the data fusion method for improving measurement accuracy. As mention in Xu et al. (2017), another benefit of this method is to effectively widen the frequency bandwidth, which is demonstrated through Fig. 13. Bridge vibration signals at one-quarter span measured using the QA accelerometer in the ambient condition and in Run 2 were analysed using Welch's method to identify modal frequency information. The corresponding auto-spectral densities (ASDs) are indicated in Fig. 13 (b) and (d). According to ambient data in Fig. 13 (b), the first two bridge vibration modes are at 9.56 Hz and 12.50 Hz. Instead of presenting two sharp peaks as in (b), the ASD of the acceleration signal in Run 2 carries high energy in the frequency range between 8.3 Hz and 12.6 Hz and captures a sharp peak at 15.31 Hz that is not observed from the ambient result in (b). This variation is due to the varying dynamic characteristics of the coupled system of train and bridge, since the total mass of the locomotive and tender exceeds 100 t. Fig. 13 (e) and (f) are the GoPro displacement measurement ('Corrected') and estimates ('Corrected + Fusion') in Run 2 as well as the corresponding ASDs. The GoPro displacement data with the sample rates of 24 Hz only carry an artificial mode at

5.53 Hz while displacement estimates after data fusion carry high energy near the first modal frequency (9.56 Hz) and identify a very small peak at 15.31 Hz that is less distinctive as in (d).

Analysis results indicate that the data fusion can widen the frequency bandwidth of displacement data. However, displacement data after data fusion also carry very high energy in the lower-frequency parts (e.g. $\leq$ 5 Hz) that could be misunderstood. Thus, the dynamic information of this bridge is better suited to measure using accelerometers.

***Displacement estimates in Run 3***

The data in Run 2 validate the accuracy improvement for vision-based monitoring through integration with acceleration data. In fact, the direct measurement by a single GoPro system in Run 2 represents a satisfactory signal-to-noise ratio and could still capture the displacement amplitude with acceptable accuracy.

Data recorded in a more challenging test condition was chosen for further study of the working performance of the mixed system. In Run 3, apparent camera shake is observed in the recorded GoPro video and the lighting condition was poor compared with that in Run 2. Sample frames in Run 2 and 3 are indicated in Fig. 14(a) and (b). The ROI T00 tracked for camera motion correction has very low contrast in Run 3, which indicates a poor measurement resolution. Also, the maximum deflection at bridge mid-span is lower than half of that in Run 2, hence requiring a better accuracy for satisfactory measurement data.

The displacement measurement and estimates at mid-span in Run 3 are indicated in Fig. 15. The measurement noise is acquired by subtracting the Imetrum DMS reference data (interpolated to the same sample rate) in Fig. 15(b). In the raw measurement, some low-frequency drift and shaking are observed from 2 s to 5 s with the maximum deviation reaching 1 mm. Considering camera motion correction provides no improvement due to poor tracking resolution for the target T00, but instead, the RMS of the measurement difference increases from 0.34 mm (‘Raw’) to 0.42 mm (‘Corrected’). For the ‘Corrected’ signal, the maximum displacement is measured as 3.93 mm, 35% higher than the reference and the cross-correlation coefficient evaluated by the reference data is 92.1%. Thus, both the displacement amplitude and the time histories measured directly by the GoPro system have poor accuracy level and are improper for bridge condition evaluation.

Through fusion of displacement ('Corrected') and acceleration data, the maximum deflection during the train passage is estimated as 2.95 mm while the reference measurement is 2.92 mm. The cross-correlation coefficient between the displacement estimate and the reference reaches 99.4% and the RMS of measured difference decreases from 0.42 mm ('Corrected') to 0.12 mm ('Corrected + Fusion').

A detailed comparison of displacement data is summarised in Table 4. Results indicate that the data fusion method is effective to provide accurate estimates of bridge deformation even when the direct measurement from the sole camera system is unsatisfactory.

**Estimation of bridge influence line**

Displacement data are an important aid for bridge condition evaluation such as identifying influence lines (IL), estimating axle loads, tying into model calibration and updating, etc. This section demonstrates one application example of measured data, i.e. estimating the bridge IL.

Run 3 involving the passage of a diesel train is taken for analysis since steam trains (including a locomotive and a tender) in the other two runs have high uncertainty on weights and axle weight distributions. The diesel train (British Rail Class 115) in Run 3 includes three four-axle carriages with each carriage length 19.50 m. The weights for the three carriages are approximately 39 tons, 30 tons and 39 tons, respectively according to manufacturer specification and are assumed to be evenly distributed to car axles for each unit. The axle locations in the front car unit are indicated in Fig. 16.

Positions of moving axles are necessarily synchronised in time with bridge response records. From the GoPro video records, the time steps when the train front and rear passed the one-quarter span point are counted to be 2.53 s and 8.91 s, respectively. Given the total train length (60.30 m), the passing speed is estimated as 34.0 km/h, and this could be used to determine time-varying positions of each axle.

Bridge girders on two sides are of the same length ($L$=14.7 m) but as shown in Fig. 4(a), the north girder on the monitoring side is shifted back by 7.15 m along the longitudinal direction due to the bridge skew. Thus, the valid load locations $X$ on the bridge vary from -7.15 m to 14.7 m.

Bridge displacement IL is related to time series of displacement data, train axle weights and locations expressed in a linear equation,

$$\mathbf{Au} = \mathbf{b} \tag{1}$$

where $\mathbf{b}$ denotes the time series of displacement data with the size $T \times 1$; $\mathbf{u}$ is a $M \times 1$ vector containing IL ordinate of the bridge that is divided into $M$ elements ($M$ = 50); and the matrix $\mathbf{A}$ with the dimension $T \times M$ involves the axle weight and location information and the matrix element $\mathbf{A}_{ij}$ corresponds to the axle load value implemented on the bridge element $j$ at the time step $i$. Providing the matrices $\mathbf{A}$ and $\mathbf{b}$, the IL ordinate $\mathbf{u}$ could be determined directly by solving $\mathbf{Au} = \mathbf{b}$.

Displacement IL ordinate at the north mid-span is presented in Fig. 17. The maximal displacement at bridge mid-span under a moving unitary force (1 N) is achieved at the location $X$ = 5.61 m with the value reaching 1.33e-5 mm.

In Fig. 17, the considered load locations ($X$) in the horizontal axis of the figure are from -7.15 m to 14.7 m. The range $X < 0$ m corresponds to the periods when the unitary force enters the south girder of this skew bridge but is not directly imposed on the north girder on the monitoring side. The bridge north mid-span starts to deform from the load position $X = -2.2$ m due to the cross beams linking two side girders. The IL ordinate in the range $X < -2.2$ m is expected to stay at zero but actually has small drifts especially when $X < -4$ m. This artificial error is possibly due to small drift error remaining in displacement data even though camera motion correction is deployed.

This section demonstrates the viability of the proposed mixed system for bridge IL estimation. One advantage of this system compared with other alternatives is that bridge responses and axle locations are derived from the same video records with no need for the time synchronisation.

## Conclusion

A vision-based monitoring system based on using a single consumer-grade camera could provide accurate characterisation of bridge deformation via displacement measurement in favourable test conditions. These would include choosing salient target patterns for tracking and avoiding any camera shake. The RMS of measurement noise at the camera-to-target distance of 6.9 m is less than 0.2 mm in this example.

An effective way to correct the influence of camera shake is by tracking the nominal motion of an adjacent stationary object. This method is very effective to remove the low-frequency drift error, but

the measurement resolution is possibly reduced considerably by tracking the low-contrast feature target on stationary objects, even leading to poorer measurement accuracy after the correction. A criterion for camera stability evaluation is proposed in this study based on the tracked motions of a stationary target and the correction is performed only when necessary.

To overcome the limitation of a sole camera system, a feasible method is to fuse the vision-based displacement measurement with acceleration data for noise reduction. The data fusion method is capable of de-noising the measurement and providing better estimates of displacement. It works well even when the camera records involve apparent camera shake and low-contrast target patterns. Thus, a mixed system consisting of a camera and an accelerometer overcomes some field testing limitations of vision-based monitoring and has potential for accurate and robust displacement sensing on bridge structures.

The mixed system is demonstrated to be effective for estimating bridge influence line, indicating the application potential for bridge condition assessment.

## Acknowledgments

We would like to thank the West Somerset Railway for permission to use their bridges and for assistance they provided. Also thanks to Karen Faulkner for the support in the field testing. Finally, the authors would like to thank the two anonymous reviewers for their constructive comments.

## References

Brownjohn, J. M. W., Koo, K.-Y., Scullion, A., and List, D. (2015). "Operational deformations in long-span bridges." *Structure and Infrastructure Engineering*, Taylor & Francis, 11(4), 556–574.

Brownjohn, J. M. W., Xu, Y., and Hester, D. (2017). "Vision-Based Bridge Deformation Monitoring." *Frontiers in Built Environment*, 3, 1–16.

Casciati, F., and Fuggini, C. (2009). "Engineering vibration monitoring by GPS: long duration records." *Earthquake Engineering and Engineering Vibration*, 8(3), 459–467.

Chang, C. C., and Xiao, X. H. (2010). "An integrated visual-inertial technique for structural displacement and velocity measurement." *Smart Structures and Systems*, 6(9), 1025–1039.

Chen, J. G., Davis, A., Wadhwa, N., Durand, F., Freeman, W. T., and Buyukozturk, O. (2017). "Video Camera-Based Vibration Measurement for Civil Infrastructure Applications." *Journal of Infrastructure Systems*, 23(3), 11.

Ehrhart, M., and Lienhart, W. (2015). "Monitoring of Civil Engineering Structures using a State-of-the-art Image Assisted Total Station." *Journal of Applied Geodesy*, 9(3), 174–182.

Feng, D., and Feng, M. Q. (2017). "Experimental validation of cost-effective vision-based structural health monitoring." *Mechanical Systems and Signal Processing*, Elsevier, 88, 199–211.

Feng, M. Q., Fukuda, Y., Feng, D., and Mizuta, M. (2015). "Nontarget Vision Sensor for Remote Measurement of Bridge Dynamic Response." *Journal of Bridge Engineering*, 20(12), 4015023.

Guizar-Sicairos, M., Thurman, S. T., and Fienup, J. R. (2008). "Efficient subpixel image registration algorithms." *Optics Letters*, 33(2), 156–158.

Hester, D., Brownjohn, J., Bocian, M., and Xu, Y. (2017). "Low cost bridge load test: Calculating bridge displacement from acceleration for load assessment calculations." *Engineering Structures*, 143, 358–374.

Hoag, A., Hoult, N. A., Take, W. A., Moreu, F., Le, H., and Tolikonda, V. (2017). "Measuring displacements of a railroad bridge using DIC and accelerometers." *Smart Structures and Systems*, 19(2), 225–236.

Hong, Y. H., Lee, S. G., and Lee, H. S. (2013). "Design of the FEM-FIR filter for displacement reconstruction using accelerations and displacements measured at different sampling rates." *Mechanical Systems and Signal Processing*, 38(2), 460–481.

Khuc, T., and Catbas, F. N. (2017). "Completely contactless structural health monitoring of real-life structures using cameras and computer vision." *Structural Control and Health Monitoring*, 24(1), e1852.

Kim, J., Kim, K., and Sohn, H. (2014). "Autonomous dynamic displacement estimation from data fusion of acceleration and intermittent displacement measurements." *Mechanical Systems and Signal Processing*, Elsevier, 42(1–2), 194–205.

Li, Z., and Chang, C. C. (2013). "Adaptive Quanti fi cation of Noise Variance Using Subspace Technique." *Journal Of Engineering Mechanics*, 139(4), 469–478.

563 Liao, W. Y., Chen, W. H., Ni, Y. Q., and Xia, Y. (2010). "Development of a vision-based real-time
564 displacement measurement system for Guangzhou New TV Tower." *Proceedings of the 5th*
565 *European Workshop on Structural Health Monitoring*, F. Casciati and Giordano M., eds., Sorrento,
566 Naples, Italy, 450–455.
567 Lou, P., Nassif, H., and Su, D. (2017). "Impact of Heavy Freight Railcar on the Remaining Fatigue Life
568 of Centenarian Railway Bridges." *Journal of Bridge Engineering*, 22(11), 4017097.
569 Macdonald, J. H. G., Dagless, E. L., Thomas, B. T., and Taylor, C. A. (1997). "Dynamic measurements
570 of the Second Severn Crossing." *Proceedings of the Institution of Civil Engineers - Transport*,
571 123(4), 241–248.
572 Martins, L. L., Rebordão, J. M., and Ribeiro, A. S. (2015). "Structural observation of long-span
573 suspension bridges for safety assessment: implementation of an optical displacement
574 measurement system." *Journal of Physics: Conference Series*, 588(1), 12004.
575 McCormick, N., Waterfall, P., and Owens, A. (2014). "Optical imaging for low-cost structural
576 measurements." *Proceedings of the Institution of Civil Engineers - Bridge Engineering*, 167(1),
577 33–42.
578 Moreu, F., Jo, H., Li, J., Kim, R. E., Cho, S., Kimmle, A., Scola, S., Le, H., Spencer, B. F., and LaFave,
579 J. M. (2015). "Dynamic Assessment of Timber Railroad Bridges Using Displacements." *Journal*
580 *of Bridge Engineering*, 20(10), 4014114.
581 Moschas, F., Psimoulis, P. A., and Stiros, S. C. (2013). "GPS / RTS data fusion to overcome signal
582 deficiencies in certain bridge dynamic monitoring projects." *Smart Structures and Systems*, 12(3),
583 251–269.
584 Murray, C., Hoag, A., Hoult, N. A., and Take, W. A. (2015). "Field monitoring of a bridge using digital
585 image correlation." *Proceedings of the Institution of Civil Engineers - Bridge Engineering*, 168(1),
586 3–12.
587 Nickitopoulou, A., Protopsalti, K., and Stiros, S. (2006). "Monitoring dynamic and quasi-static
588 deformations of large flexible engineering structures with GPS: Accuracy, limitations and
589 promises." *Engineering Structures*, 28(10), 1471–1482.
590 Park, J.-W., Moon, D.-S., Yoon, H., Gomez, F., Spencer Jr., B. F., and Kim, J. R. (2018). "Visual-

591 inertial displacement sensing using data fusion of vision-based displacement with acceleration."
592 *Structural Control and Health Monitoring*, 25(3), e2122.
593 Ribeiro, D., Calçada, R., Ferreira, J., and Martins, T. (2014). "Non-contact measurement of the dynamic
594 displacement of railway bridges using an advanced video-based system." *Engineering Structures*,
595 75, 164–180.
596 Schreier, H., Orteu, J.-J., and Sutton, M. A. (2009). *Image Correlation for Shape, Motion and*
597 *Deformation Measurements*. Springer US, Boston, MA.
598 Smyth, A., and Wu, M. (2007). "Multi-rate Kalman filtering for the data fusion of displacement and
599 acceleration response measurements in dynamic system monitoring." *Mechanical Systems and*
600 *Signal Processing*, 21(2), 706–723.
601 Stephen, G. A., Brownjohn, J. M. W., and Taylor, C. A. (1993). "Measurements of static and dynamic
602 displacement from visual monitoring of the Humber Bridge." *Engineering Structures*, Elsevier,
603 15(3), 197–208.
604 Sukkarieh, S. (2000). "Low cost, high integrity, aided inertial navigation systems for autonomous land
605 vehicles." University of Sydney.
606 Wang, N., O'Malley, C., Ellingwood, B. R., and Zureick, A.-H. (2011). "Bridge Rating Using System
607 Reliability Assessment. I: Assessment and Verification by Load Testing." *Journal of Bridge*
608 *Engineering*, 16(6), 854–862.
609 Xu, Y., Brownjohn, J., Hester, D., and Koo, K. Y. (2016). "Dynamic displacement measurement of a
610 long span bridge using vision-based system." *8th European Workshop On Structural Health*
611 *Monitoring (EWSHM 2016)*, Bilbao, Spain.
612 Xu, Y., Brownjohn, J., and Kong, D. (2018). "A non-contact vision-based system for multipoint
613 displacement monitoring in a cable-stayed footbridge." *Structural Control and Health Monitoring*,
614 e2155.
615 Xu, Y., and Brownjohn, J. M. W. (2018). "Vision-based systems for structural deformation
616 measurement: case studies." *Proceedings of the Institution of Civil Engineers - Structures and*
617 *Buildings*, 1–45.
618 Xu, Y., Brownjohn, J. M. W., Hester, D., and Koo, K. Y. (2017). "Long-span bridges: Enhanced data

fusion of GPS displacement and deck accelerations." *Engineering Structures*, 147, 639–651.

Yoneyama, S., and Ueda, H. (2012). "Bridge Deflection Measurement Using Digital Image Correlation with Camera Movement Correction." *Materials Transactions*, 53(2), 285–290.

## Figures

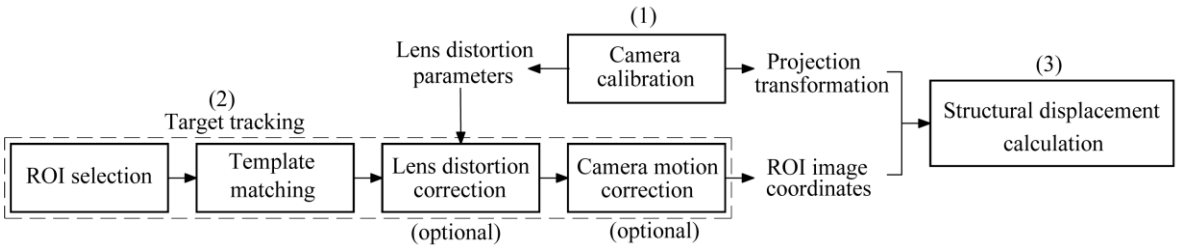


Fig. 1. Flowchart of video processing procedures

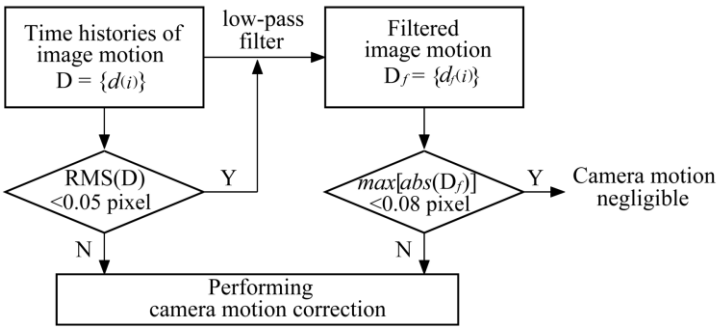


Fig. 2. Evaluation criteria for camera stability condition

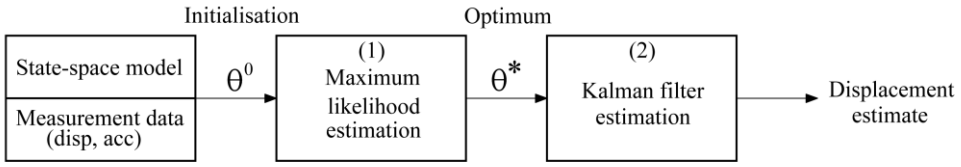


Fig. 3. Procedures of data fusion

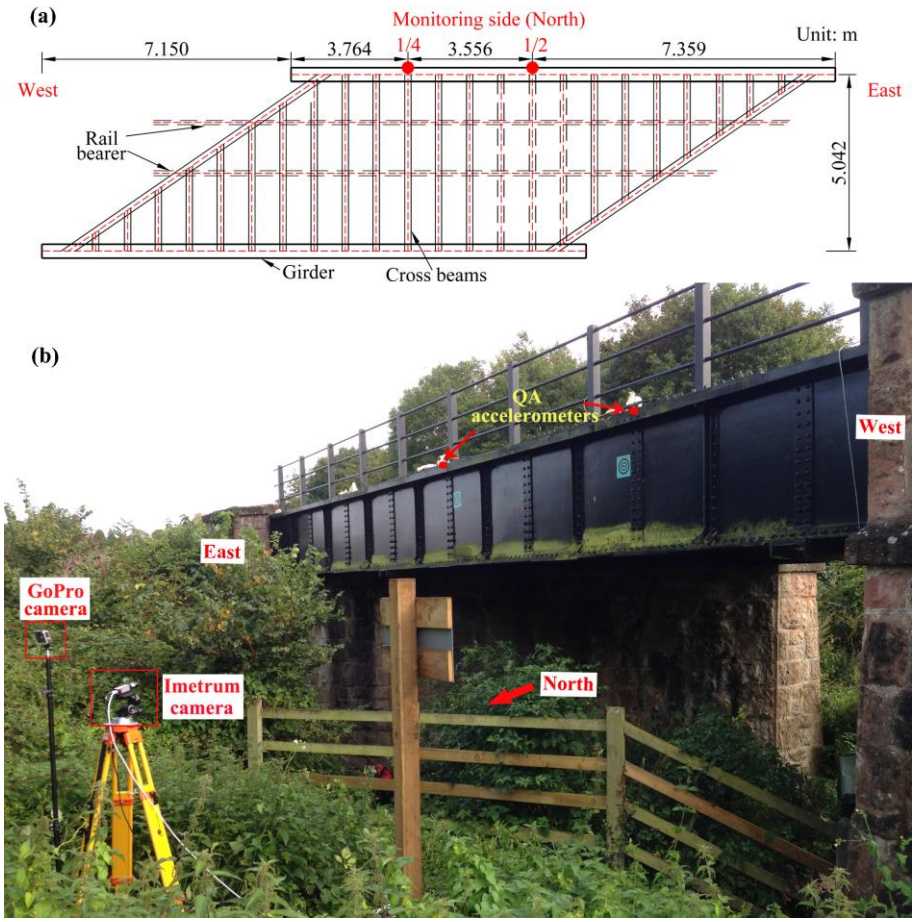


Fig. 4. Bridge plan (a) and sensor locations (b)


Fig. 5. One sample frame by the GoPro camera before and after removing lens distortion: (a) before correction; and (b) after correction.

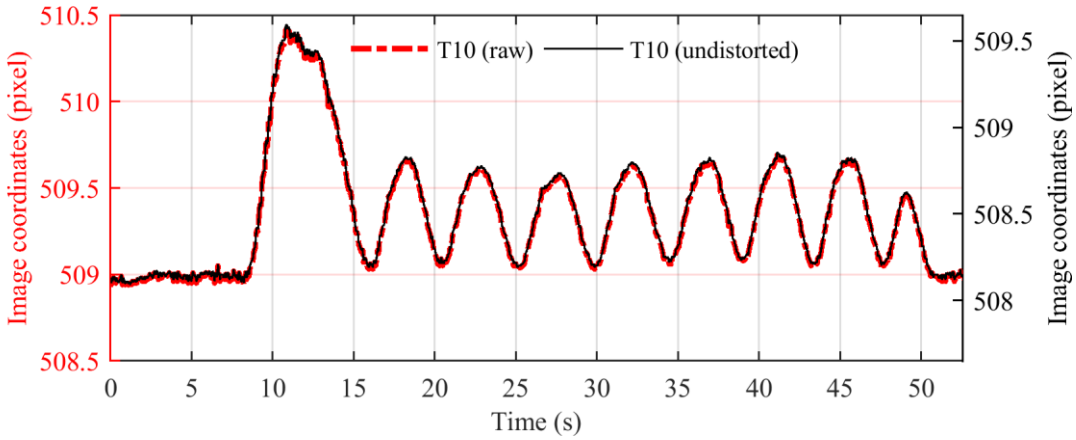


Fig. 6. Time series of image coordinates for the target T10 along image height direction before and after removing lens distortion influence

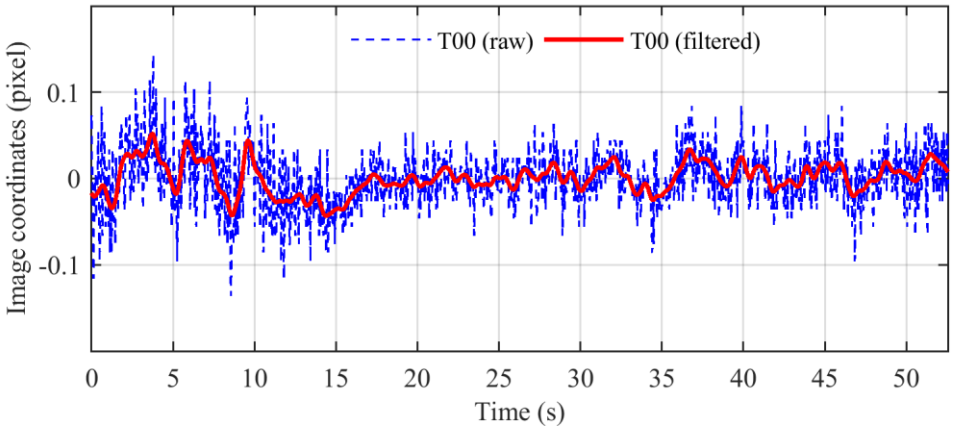


Fig. 7. Time series of image motions for the target T00 along image height direction

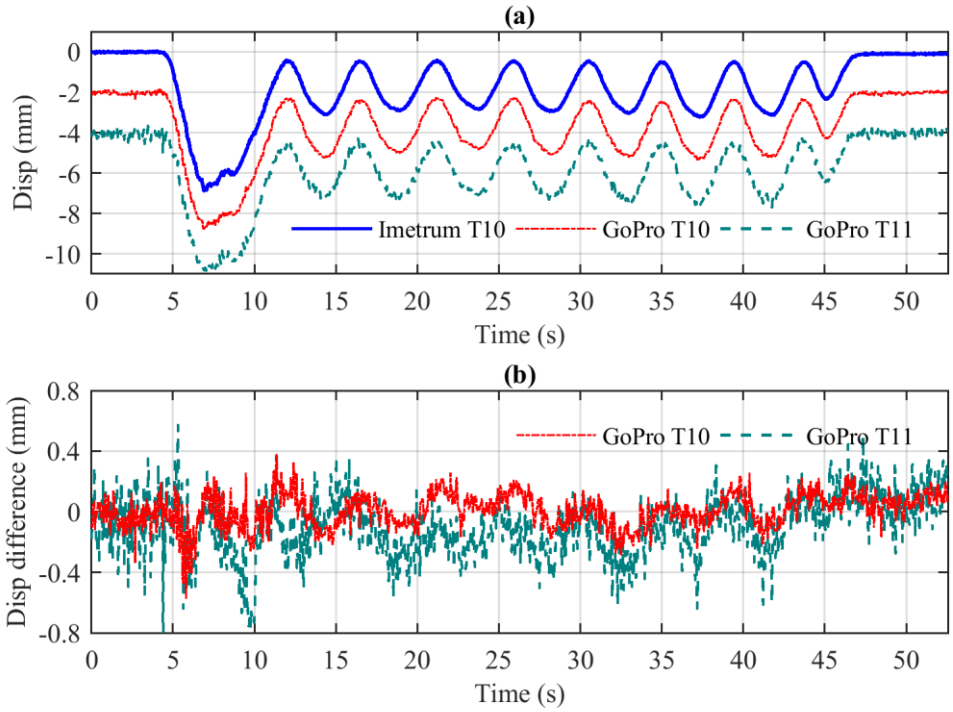


Fig. 8. Measured displacement in the vertical direction at bridge mid-span by two vision-based systems: (a) displacement measurement (curves are shifted along y axis for clarification); and (b) the GoPro measurement error evaluated by the reference Imetrum DMS

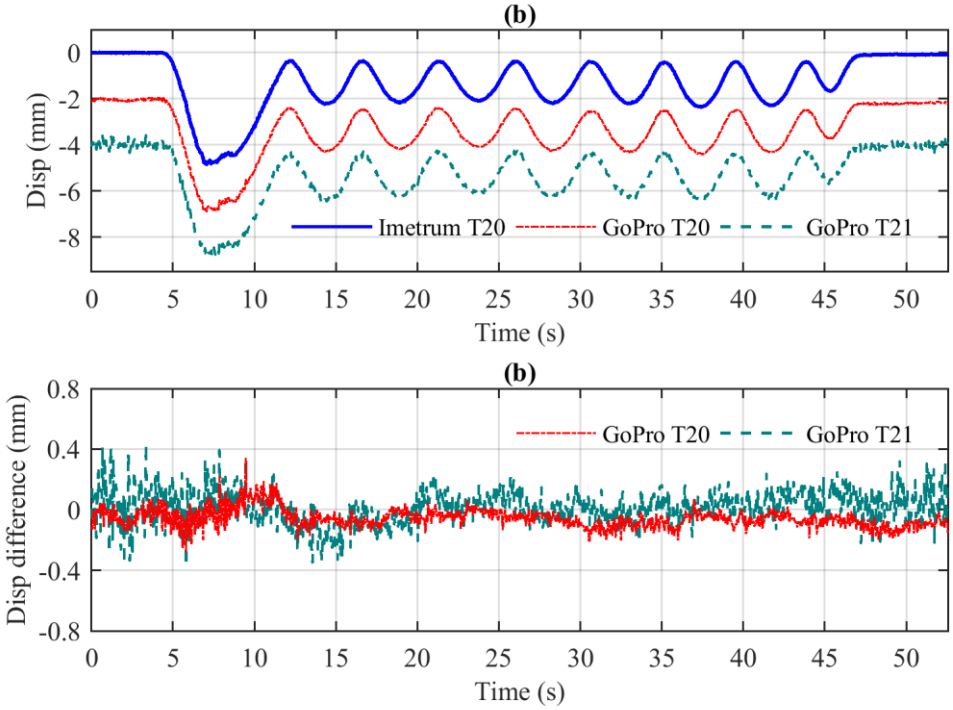


Fig. 9. Measured displacement in the vertical direction at bridge one-quarter span by two vision-based systems: (a) displacement measurement (curves are shifted along y axis for clarification); and (b) the GoPro measurement error evaluated by the reference Imetrum DMS

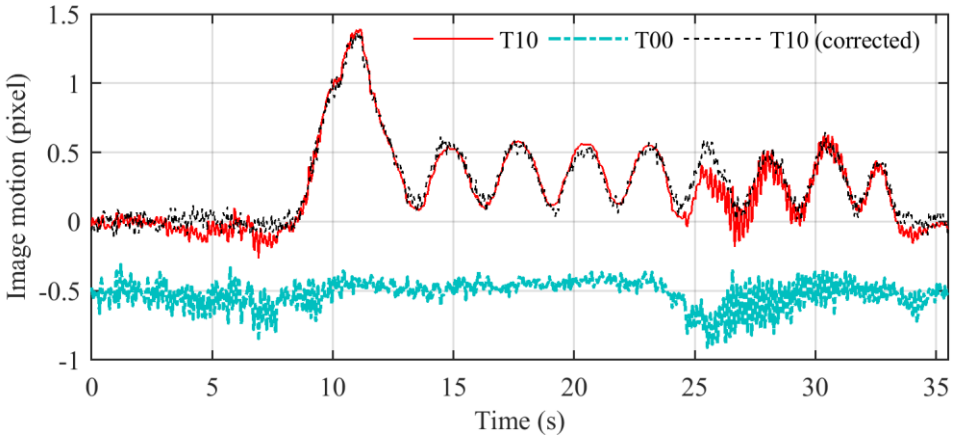


Fig. 10. Time histories of image motions for the target T10 along the image height direction before and after camera motion correction (curves are shifted along y axis for clarification)

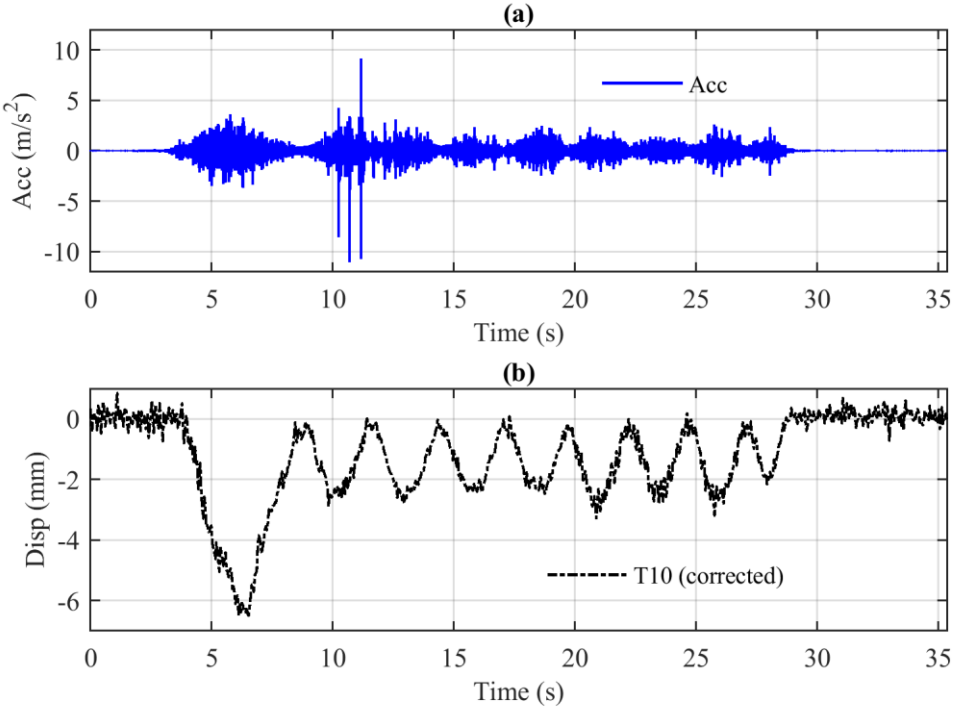


Fig. 11. Time histories of accelerometer and GoPro displacement data in Run 2 at mid-span in vertical direction: (a) accelerometer measurement; and (b) displacement measurement by the GoPro system.

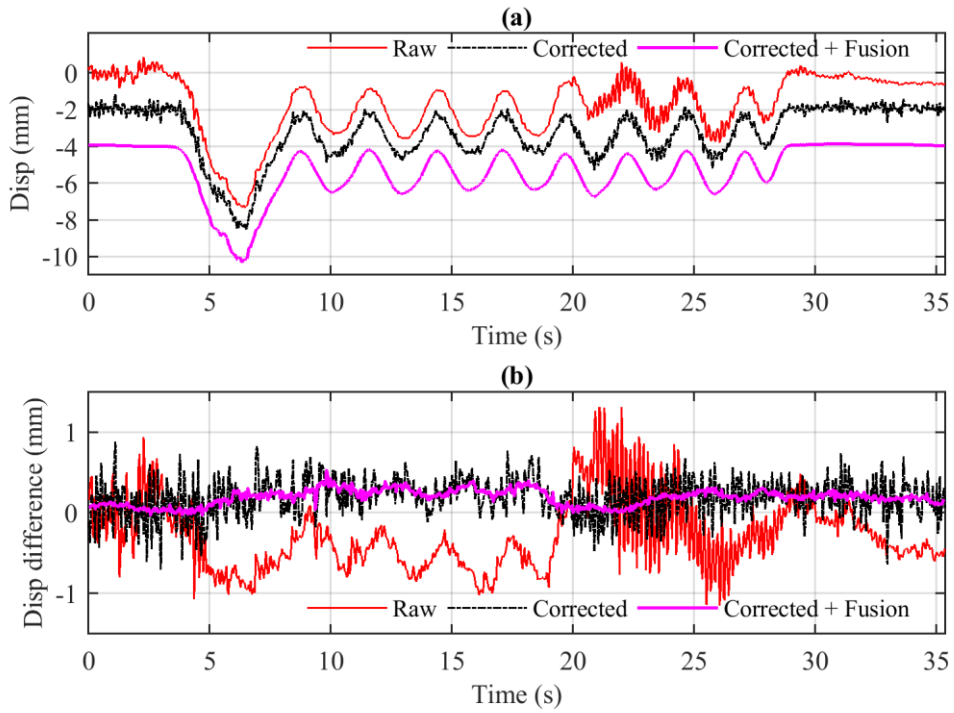

Fig. 12. Time histories of displacement measurement and estimates for T10 in the vertical direction in Run 2: (a) displacement measurement and estimates (curves are shifted along y axis for clarification); and (b) measurement or estimation error compared with the reference Imetrum DMS

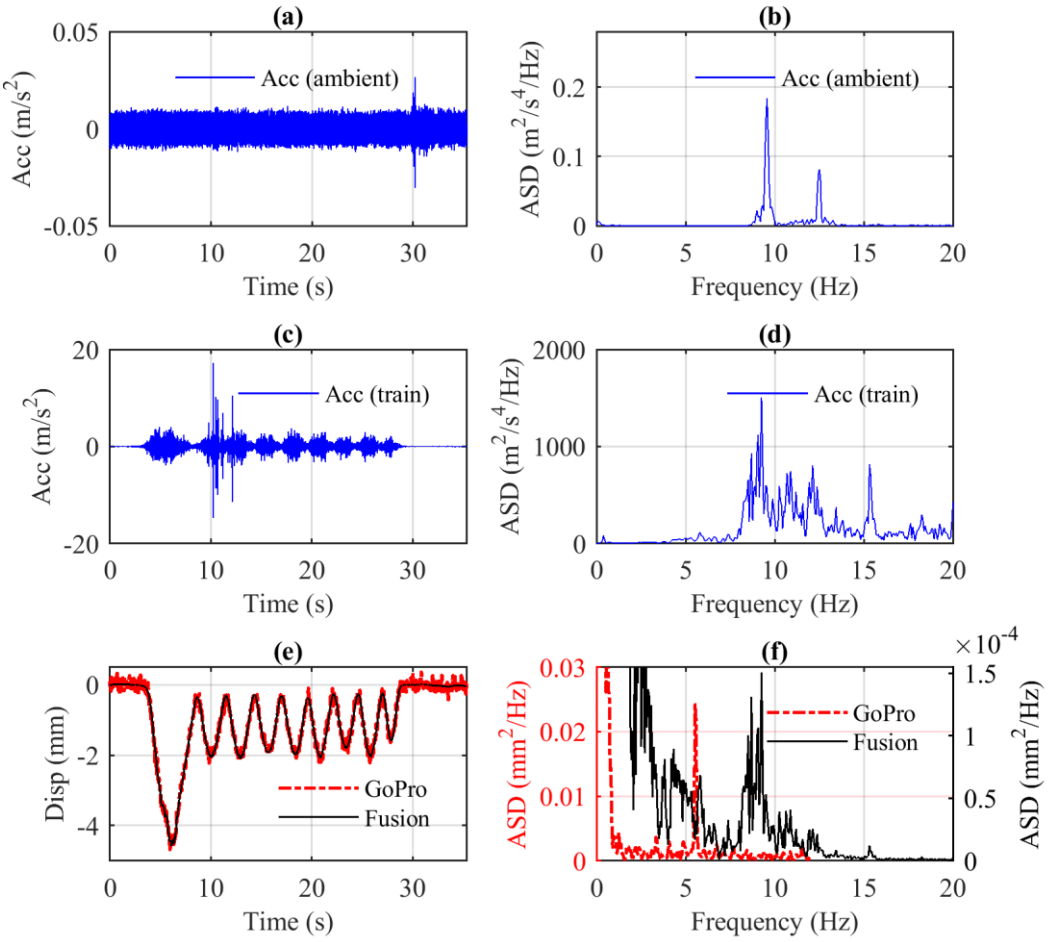


Fig. 13. Time series and auto-spectral densities (ASDs) of accelerometer measurement and of displacement measurement and estimates in Run 2: (a) accelerometer data in ambient condition; (b) the ASD of the data in (a); (c) accelerometer data in Run 2; (d) the ASD of the data in (c); (e) displacement data in Run 2; and (f) the ASD of the data in (e).

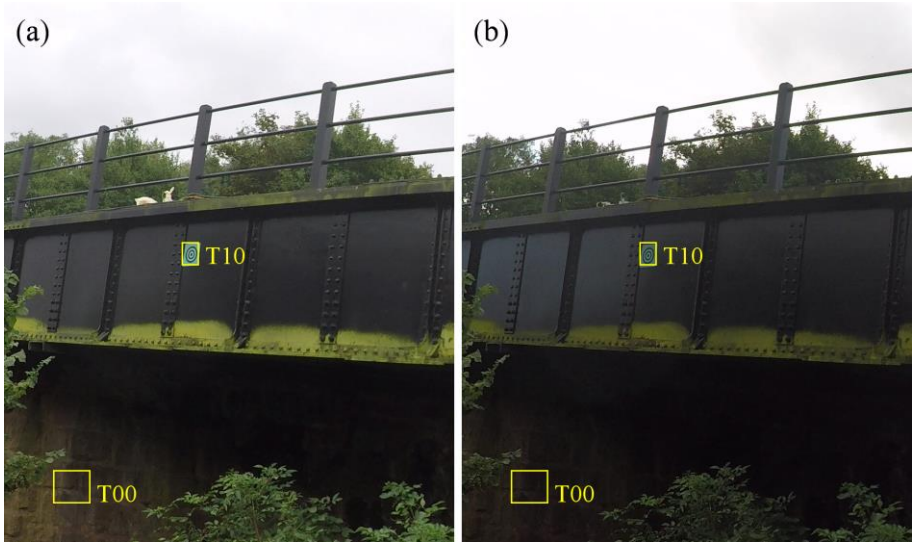


Fig. 14. Sample frames with marked locations of ROIs T01and T10 in Run 2 (left) and Run 3 (right)

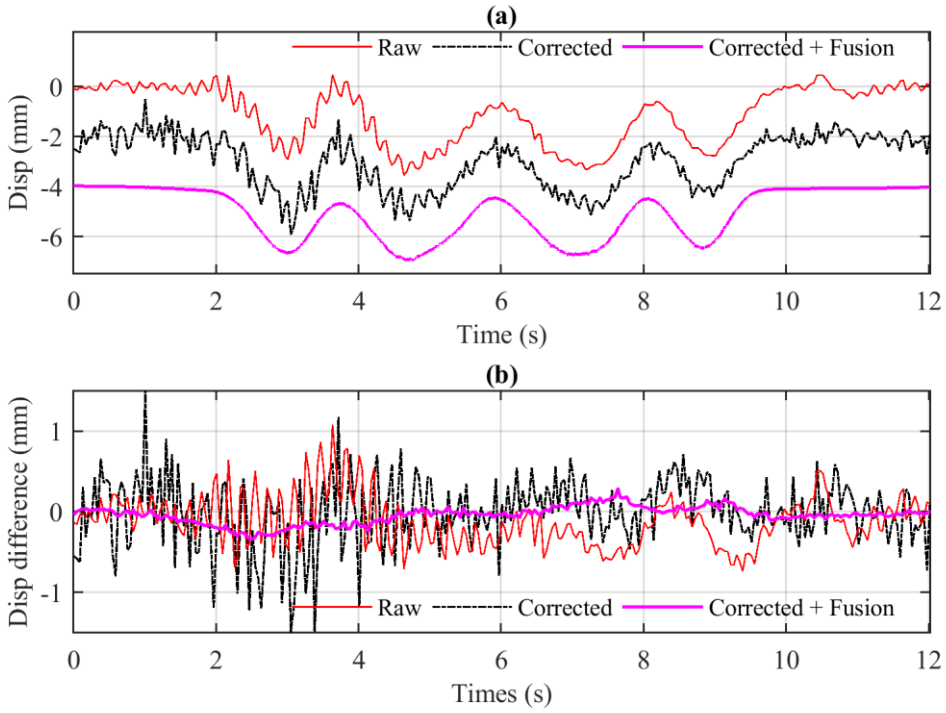


Fig. 15. Time histories of displacement measurement and estimates for T10 in the vertical direction in Run 3: (a) displacement measurement and estimates (curves are shifted along y axis for clarification); and (b) measurement or estimation error compared with the reference Imetrum DMS

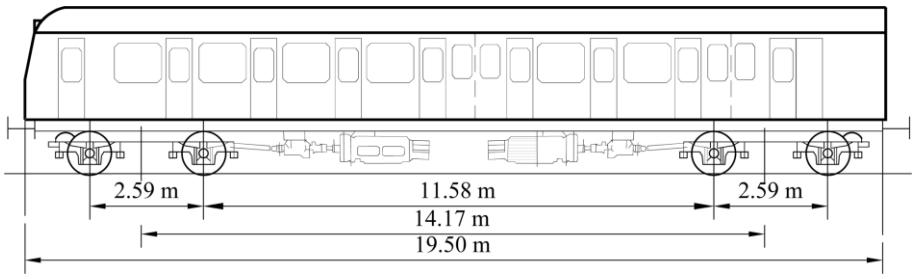


Fig. 16. Diagram of the first carriage in the diesel train passed in Run 3

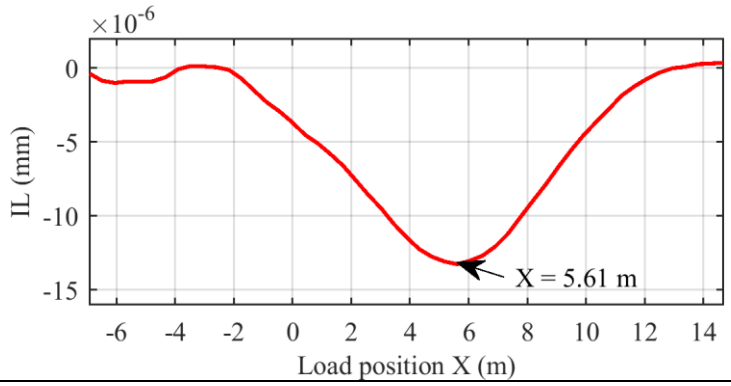


Fig. 17. Displacement influence line (IL) at bridge north mid-span under a moving unitary force (1 N)

## Tables

Table 1. Record information about three runs involving train passages

| Run # | Train type | No. of carriages | Train speed (km/h) | Maximum deflection | GoPro videos involving camera shake |
|---|---|---|---|---|---|
| Run 1 | Steam train | 8 | 16 | 6.87 mm | No |
| Run 2 | Steam train | 8 | 27 | 6.51 mm | Yes |
| Run 3 | Diesel train | 3 | 34 | 2.92 mm | Yes |

Table 2. Evaluation of measurement noise during the stationary periods in Run 1

| RMS of noise (mm) | Artificial targets | | Natural patterns | |
|---|---|---|---|---|
| | T10 | T20 | T11 | T21 |
| Imetrum DMS | 0.02 | 0.01 | -- | -- |
| GoPro | 0.07 | 0.04 | 0.16 | 0.14 |

Table 3. Evaluation of three displacement signals for the natural target T11 at mid-span and for the artificial target T20 at one-quarter span through comparison with the reference Imetrum DMS in Run 2

| Displacement signals | T11 | | | T20 | | |
|---|---|---|---|---|---|---|
| | Maximum displacement (mm) | Cross-correlation coefficients | RMS of difference (mm) | Maximum displacement (mm) | Cross-correlation coefficients | RMS of difference (mm) |
| Reference | 6.51 | -- | -- | 4.57 | -- | -- |
| Raw | 6.92 | 96.5% | 0.46 | 4.96 | 97.9% | 0.29 |
| Corrected | 6.61 | 98.4% | 0.35 | 4.68 | 99.2% | 0.13 |
| Corrected + Fusion | 6.38 | 99.7% | 0.24 | 4.57 | 99.9% | 0.05 |

Table 4. Evaluation of three displacement signals for the target T10 at mid-span through comparison with the reference Imetrum DMS in Run 3

| Displacement signals | Maximum displacement (mm) | Cross-correlation coefficients | RMS of difference (mm) |
|---|---|---|---|
| Reference | 2.92 | -- | -- |
| Raw | 3.55 | 96.5% | 0.34 |
| Corrected | 3.93 | 92.1% | 0.42 |
| Corrected + Fusion | 2.95 | 99.4% | 0.12 |